PRE-FLIGHT VERIFICATION OF THE CUBESAT ATTITUDE CONTROL SYSTEM FOR THE QUBE MISSION

Lisa Elsner [(1)], Timon Petermann [(1)], Maximilian von Arnim [(1)], Klaus Schilling [(1)]

[(1)] Zentrum für Telematik (ZfT), Magdalene-Schoch-Str. 5 Würzburg, Germany
{firstname.lastname}@telematik-zentrum.de

ABSTRACT

Quantum key encoding guarantees secure communication networks. Nevertheless, for global communication networks the quantum key distribution (QKD) over larger distances is currently only possible through optical links via satellites. The challenge for the satellite is the high precision pointing towards the terrestrial target antennas, especially with cost-efficient small satellites. For the nano-satellite class of a few kilograms, related attitude control approaches and test procedures had to be developed. This paper presents the attitude determination and control system (ADCS) design of the QUBE-1 mission. During a quantum cryptography experiment, its Fine Pointing mode uses a star tracker and gyroscopes to track the ground station with the optical payload. Its distributed sensor data processing increases fault tolerance and reliability. To verify the ADCS' performance, we rely on a distributed hardware-in-the-loop (HIL) test environment. High-precision turntables are offering new opportunities to stimulate the satellite sensors. Through the distributed setup, a stationary star simulator completes the test environment. We show that the ADCS meets the pointing requirement in HIL tests in different scenarios. Integrating satellite software, testbeds, and simulation gives new chances for on-ground verification and exploring innovative sensor and control approaches.

1 INTRODUCTION

The demand for secure communication in global communication networks increases. Here, QKD methods offer new approaches to encryption. For QKD over large distances, satellites act as enabler [1]. The MICIUS satellite (launched in August 2016) pioneered this approach by demonstrating a secure communication between Europe and China [1]. The key is generated onboard and then downlinked by a secure optical link employing entangled photons. MICIUS was a satellite with a 631 kg mass. If smaller satellites can be used, the required multi-satellite networks benefit from a significant cost advantage. To achieve the required precision to point and track the receiving antenna with a nano-satellite of a few kilograms raised unprecedented accuracy requirements.
This contribution addresses the design of the CubeSat QUBE-1 with a mass of 3.5 kg [2] to achieve these objectives, particularly its precision attitude control system, as well as its performance tests employing innovative HIL equipment. The QUBE-1 launch is scheduled for July 2024.
The paper begins by describing the ADCS and the sensors and actuators used. We provide insights into the functionality of the various ADCS modes and focus on the Fine Pointing mode primarily investigated in this study. Following this, we describe the test environment in which the experiments took place. This section contains details about the test procedure during the development process of the ADCS with the various complexity levels and provides information about the test environment. Subsequently, we describe various test scenarios and present the corresponding results, which show the pointing accuracy of the attitude control system during the overflight. We conclude by discussing the challenges encountered, possible limitations, and opportunities for future improvements.

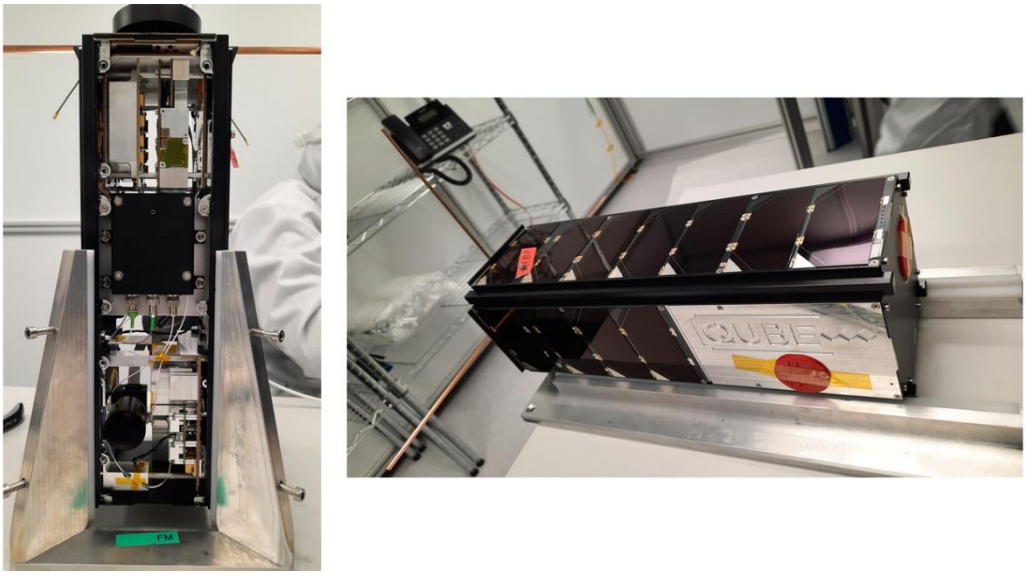

Figure 1: Completed flight model of the QUBE-1 satellite.

2 SYSTEM DESCRIPTION

QUBE-1 is dedicated to downlinking photons containing encoded quantum information for encryption key exchange [3]. Figure 1 shows the 3U pico-satellite, built according to the CubeSat design specifications. Key subsystems are placed in the lower part of the satellite, with a common backplane providing access to the UNISEC-Europe system bus, known for its reliability and cable-free design [4]. In the middle section are two quantum payloads provided by the Ludwig Maximilian University in Munich (LMU) and the Max Planck Institute for the Science of Light (MPL), connected to DLR's optical downlink system OSIRIS, placed in the upper section. Communication between subsystems and payloads is facilitated by the COMPASS protocol, offering a multi-level structure for global accessibility and a variety of shared services [5].

During the experiments, a compact quantum random number generator (QRNG) will generate sequences that will be used to configure light quantum states that are transmitted to DLR's optical ground station for analysis. The corresponding random numbers will also be transmitted via a radio downlink. By comparing the received photon states with the generated numbers, eavesdropping attempts can be easily detected due to the inherent properties of quantum mechanics. These experiments investigate the feasibility of secure communication links on a CubeSat scale.

In the initial ground station acquisition phase, the satellite has to orient with an accuracy better than 1° toward the receiving ground station antenna. After contact is established, the nested control system orients with respect to an optical beacon emitted from the ground station.

To achieve initial satellite pointing with an accuracy of 1° towards the ground station is a challenge to the ADCS at such a miniaturization level. QUBE-1 is therefore equipped with a star tracker, which is the most accurate in-space attitude sensor up-to-date at CubeSat dimensions. Miniature reaction wheels are used to track the optical ground station precisely [2].

Once the 1° pointing accuracy has been achieved, the ADCS receives the incident angles of the beacon signal from the payload, and the controller uses this information to calculate the actuator inputs. To maximize the probability of mission success, the ADCS must be intensively verified and tested on the ground, which includes calibrations and testing the complete control loop. The aim is to test the overflight as realistically as possible and to integrate as many real components as possible, in particular sensors and actuators, into the tests.

An overview of existing ADCS testbeds is presented in [5], which are divided into two main categories: testbeds based on microgravity simulation and testbeds based on external attitude

manipulation. The former uses a very thin air layer to enable almost frictionless movement. A disadvantage of such test facilities is that they are often severely limited in terms of pitch- and roll-axis rotations but allow the verification of the real actuators. In contrast, the external attitude manipulators often have extensive coverage of the permitted rotation ranges in all axes. However, a change in attitude is achieved by the external manipulator and not by the satellite's actuator itself. As the Zentrum für Telematik (ZfT) has both test facilities available, we decided to split the testing of the complete control loop in order to verify both the real sensors and real actuators. The chain from the controller to the reaction wheels was evaluated with the air bearing testbed, and the chain from sensors (gyroscope and star tracker) to the controller was verified with the external attitude manipulator, which is the focus of this paper. To perform the tests, one of the two high precision three-axis motion simulators (turntable), described in [5], was used. The controller software was extended and improved to make better use of its highly accurate angular measurements (0.36 arcsec [5]). This testbed was complemented with HIL simulation capabilities and extended to have a realistic scenario. This included the integration of a star simulator, and implementing time synchronization between turntable, satellite and (real-time) simulation software with sufficient accuracy [6].

2.1 ATTITUDE DETERMINATION AND CONTROL SYSTEM

The QUBE-1 ADCS is equipped with several components to determine and control the satellite's orientation. It comprises four CMOS-based Sun sensors, six inertial measurement units (IMUs), including magnetometers, and a star tracker for highly precise attitude determination. As actuators, it includes five magnetorquers and six miniaturized reaction wheels, two per axis. The Sun sensors, IMUs and torquers are located on the spacecraft panels with a dedicated microcontroller unit (MCU) on each panel, optimizing computational efficiency. The ADCS subsystem employs two single-core MCUs for redundancy and utilizes a real-time operation system (RTOS) to ensure timely execution of control loops. This integrated system collectively facilitates accurate and robust satellite attitude control, crucial for meeting the required pointing accuracy. The ADCS has five different modes: Detumbling, Sun Pointing, Safety, Coarse and Fine Pointing mode, as shown in Figure 2.

The purpose of the Detumbling mode is to bring the satellite from a wide range of initial conditions, including high-speed tumbling motions, to a stable condition where the satellite's rotation rate stays within a specified range that allows ground communication with the satellite. Therefore, we implemented checks to observe the magnitude and change of rotation rates over time, as well as track sensor, controller, or actuator errors. In the control loop of the Detumbling mode, gyroscopes and magnetometers are fed as sensor inputs into a b-cross controller [7]. The torque output of the controller is distributed to the magnetorquers. The Detumbling mode serves as the default to switch to whenever one of the other modes, except Safety, reaches some defined exit condition or detects a component failure. This aims to ensure that sensors and actuators required in the main mission phase (Earth target tracking (ETT) phase) can be restored to nominal conditions autonomously, for example, to desaturate the reaction wheels. The Safety mode serves as a fallback mode in case an unrecoverable anomaly occurs during Detumbling. It runs the same control loop as in Detumbling, with the difference that in case of permanent errors, the controller and actuator will be permanently turned off until the operator from ground performs an action.

The Sun Pointing mode orients the satellite's solar panels toward the Sun to restore the satellite's state of charge after an experiment or eclipse phase. A so-called "barbecue" strategy induces a slow back-and-forth rotation around the satellite's (long) z-axis, exposing all of the solar panels to the Sun while avoiding unbalanced heating of the satellite. Additionally, the Sun Pointing mode also guarantees the safety of Sun-sensitive instruments (star tracker and payload) by actively pointing them away from the Sun. The apertures of the star tracker and the OSIRIS payload are found on the panels in positive y and z direction, respectively. Both are visible with protective red caps in Figure 1.

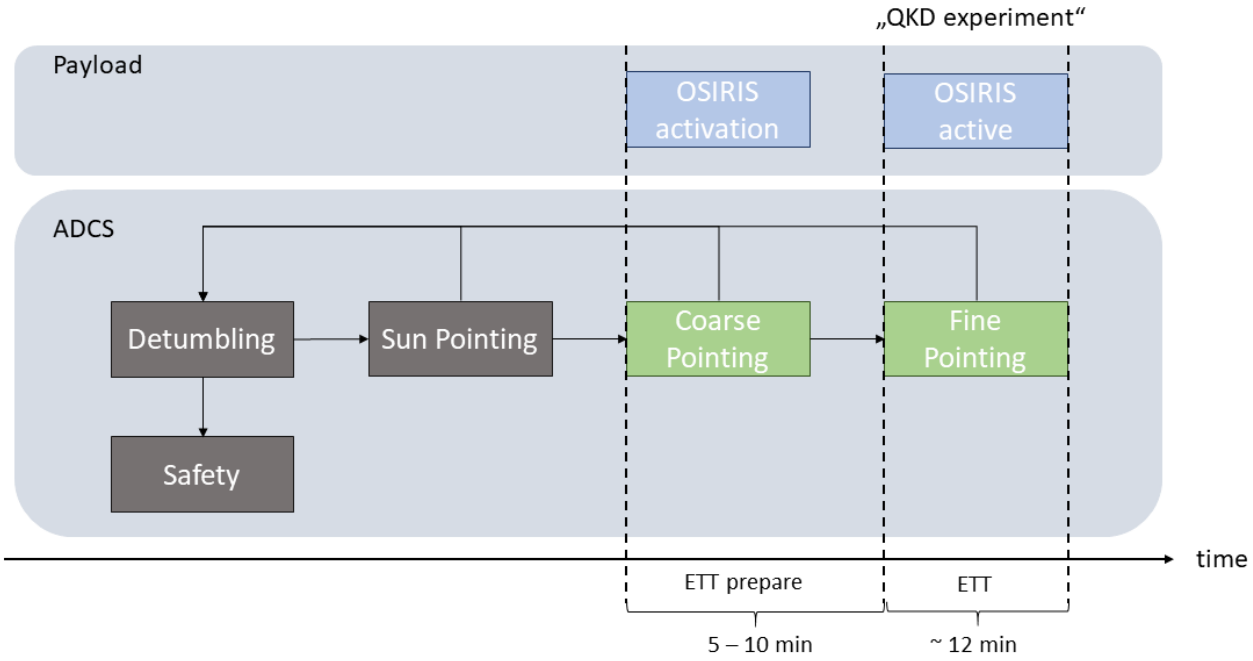

Figure 2: The ADCS modes of QUBE-1.

Short exposure, for example, while tumbling, is unproblematic, but the optical components should not stare into the Sun for long durations. Compared to tumbling, the angular velocity in this "barbecue" mode is much lower both to avoid a need for extended detumbling prior to payload operations and to respect the torque limits of the magnetorquers. Henceforth, a simple spin stabilization could expose the optical components for too long. This leaves one remaining degree of freedom for the attitude. To minimize the required rotation when switching to pointing, QUBE-1 aligns the z-axis of the body frame with the minus z-axis of the Earth-centered inertial (ECI) frame. Compared to the Detumbling mode, Sun sensors are used as additional sensor inputs to provide absolute attitude information and the controller is switched to the tracking controller [8], which is a quaternion feedback controller with hysteresis. The sensor inputs are filtered with the isotropic Kalman filter (IKF) [9], considering not only the sensor readings but also the expected Sun vector and magnetic field in the inertial frame as calculated by models based on the current location and time. The guidance in this mode calculates the required attitude of the satellite based on the current Sun direction and Earth's magnetic field.

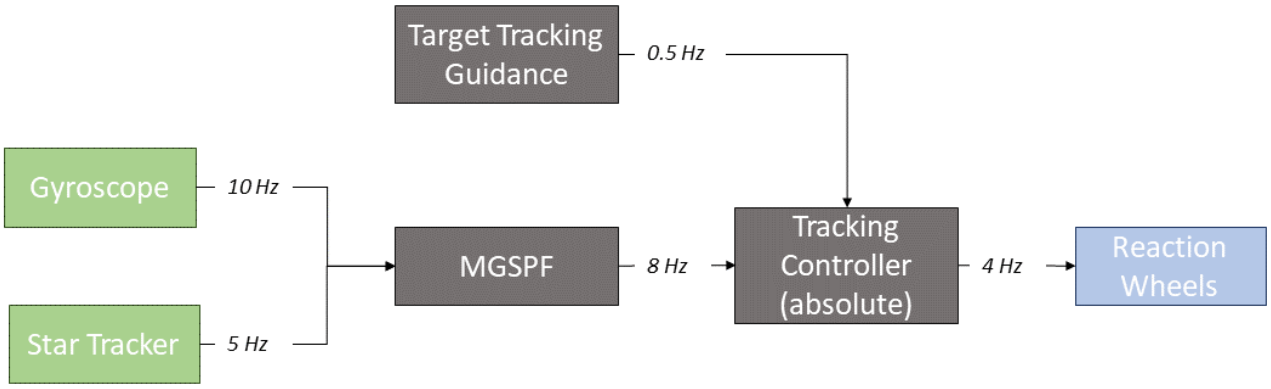

Figure 3: Processing loop of Fine Pointing mode using star tracker and gyroscope as sensor inputs.

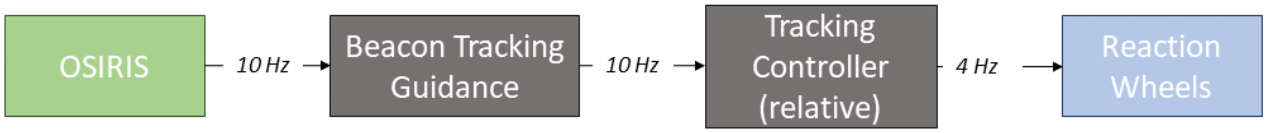

Figure 4: Processing loop of Fine Pointing mode using incident angles from OSIRIS payload as sensor inputs.

The remaining two modes, Coarse and Fine Pointing, are the two mission-specific modes where the QKD experiment is prepared and executed. This also requires turning on the payload OSIRIS, which is done during the Coarse Pointing mode. The control loop of the two modes differs only in the accuracy of the attitude determination, implying that the sensors and attitude filter are switched. The sensor set is switched from the Sun sensor, magnetometer and gyroscope to the star tracker and gyroscope; the filter is switched accordingly from the IKF to the marginal geometric sigma point filter (MGSPF) [10]. Both the sensors and the filter must indicate that they are fully initialized and ready to ensure a smooth transition. The control loop of the Fine Pointing mode is shown in Figure 2. The initial orientation towards the optical ground station will be done using the star tracker and the gyroscope as sensor inputs, as illustrated in Figure 3. The target tracking guidance provides the required attitude to track the optical ground station on Earth, which is pre-calculated on ground using systems tool kit (STK) software and stored in a file with two seconds update steps. Onboard the satellite, the file is read out and the data is interpolated linearly between the steps to provide the controller with a sufficient update rate. When generating the guidance, it is ensured that the star tracker does not have the Earth, the Sun or other disturbing celestial bodies in the field of view at any time during the overflight. As soon as the ADCS receives incident angles from OSIRIS stably, the controller automatically switches to use the relative inputs provided by the beacon tracking guidance, as shown in Figure 4. The beacon tracking guidance converts the incident angles of the optical beacon signal received by OSIRIS into a relative error that is directly fed into the controller. The actuators are also switched in the Coarse and Fine Pointing mode to use the reaction wheels.

2.2 TEST PROCEDURE

During the development and testing, our approach follows the principle of increasing complexity in each verification step. In the first step, we verified the fulfillment of the requirements in a pure processor-in-the-loop (PIL) simulation. In this step, all the sensor inputs are modeled by the simulation. In the second phase, we integrated the real sensors step-by-step. Eventually, we validated the Fine Pointing mode of the ADCS in a closed loop HIL test covering all the sensors used.
This process is illustrated in Figure 5, starting with on-desk tests with a flatsat and a high level of simulated components on the left side and finishing the engineering model (EM) in the distributed HIL testbed. In intermediate steps, tests with the complete satellite EM were performed to consider the whole system behavior (like bus traffic due to inter-subsystem or telemetry traffic).

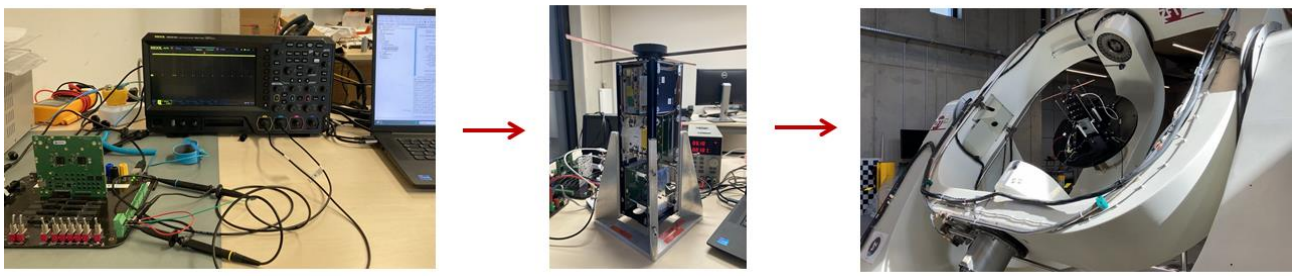

Figure 5: Test procedure with increased complexity levels. Starting in a pure flatsat with UNISEC [4] development boards and AOCS subsystem on the left in a pure PIL test. Next, the verification is performed in PIL with the complete satellite EM (center), as shown in the middle. Finally, a full HIL is performed on the turntable testbed (right).

2.2.1 PROCESSOR-IN-THE-LOOP

To test the embedded implementation of the filters and the controllers on the RTOS of the ADCS, we performed PIL simulations. This ensures that the processing loop frequency goals described in the previous section are met and that the MCU is capable of performing the required computations. For this, a real-time simulation node runs on an external PC. It is modeling the orbit as well as the attitude dynamics of the satellite in a given simulation scenario. Further, it is responsible for keeping and distributing the simulation time in the distributed testbed. For this, the simulation opens a network time protocol (NTP) server. Onboard the satellite, a simple network time protocol (SNTP) client is running that can connect to the NTP server and synchronize the satellite to the simulation time with an accuracy of about 10ms [11].

Several relevant models for the ADCS are available in our ADCS simulation framework. The framework is written in Java and builds up on Orekit [12], an open-source, state-of-the-art, space flight dynamics simulation framework with wide recognition and proven performance among competing tools. Orekit provides the orbital state including position and velocity, as well as environmental parameters such as the local magnetic field and atmospheric density or the direction towards celestial objects like the Sun. These states are input for a custom attitude dynamics model and the associated ADCS sensor and actuator models. For mathematics and statistics components, the Java library Hipparchus is used [13].

The overall structure of the PIL simulation is shown in Figure 6. On the left side, all the virtual/simulated parts are depicted. The interface from these components running on a separate PC to the actual ADCS hardware is performed via the onboard protocol COMPASS, which serves as a network and transport layer and runs independently of the underlying communications hardware. More information on COMPASS can be found in [5]. The simulation - including all simulated components - appears as a node in the COMPASS network. Simulated components can send (or receive) messages asynchronously, with a loose synchronization based only on the simulated time. From the application software on the PC, COMPASS packets are sent via USB to a development board or the satellite's onboard computer (OBC), which in turn forwards the packets to the ADCS via the satellite's inter-subsystem I2C bus according to a dynamic routing table. This way, simulated sensor data is received on the ADCS MCU as if the data would come from a panel or other subsystem. Likewise, actuator commands or controller outputs originating from the ADCS can be rerouted to the PC to become inputs for the simulated actuators.

We also used this design approach to implement virtual panels, allowing tests with the ADCS without needing panel hardware. The simulation framework comes with models for all the sensors available on QUBE-1. The gyroscopes are simulated using the discrete gyroscope model given in [7], based on the simulated rotation rate of the satellite $\overrightarrow{\omega_s}$ and parameterized by their angular random walk and the rate random walk. The magnetometer model can use a variety of parameters similar to the one given in [14], though their dominating error source after calibration is random noise [15], so the test campaign used only this to parameterize the model. For modeling the star tracker, noise is added to the propagated quaternion $\overrightarrow{q_s}$ based on the given standard deviations in and around the boresight. The output of the calibrated Sun sensors [5] is a unit vector in the body frame, pointing towards the Sun. Its errors are simulated by rotating the unit vector away from the true direction by a small random angle, which preserves the unit length property. The reaction wheels are abstracted by limiting the simulated torque to their maximum achievable torque, even if the controller demands more. Otherwise, the commanded torque is passed directly to the attitude propagator. High-fidelity reaction wheel models are implemented but considered not advantageous for the tests conducted, as such models require precise knowledge of the real wheels' behavior. Likewise, we neglected the internal dynamics of the magnetorquers for the simulation; QUBE-1's use of air coils rather than ferromagnetic cores allows this approximation.

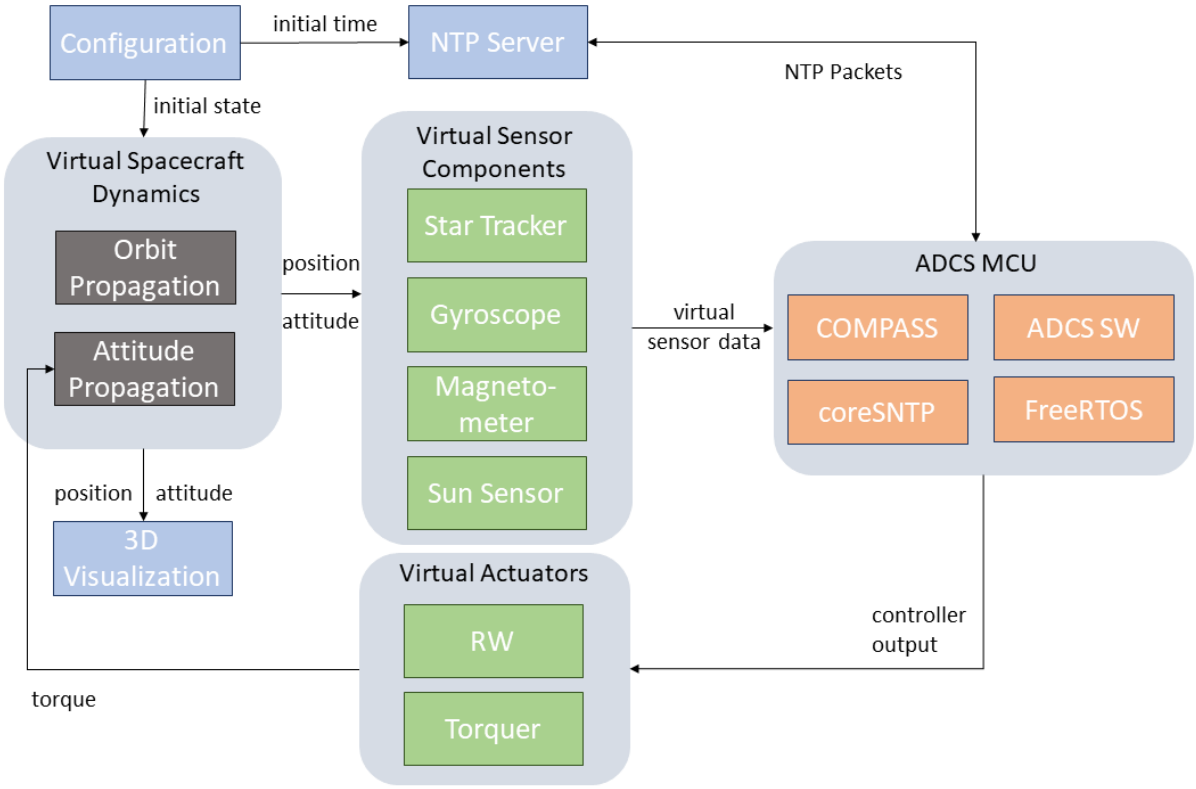

Figure 6: Testbed architecture with virtual satellite components.

2.2.2 HARDWARE-IN-THE-LOOP WITH DISTRIBUTED TESTBED

In extension to the PIL simulations, the actual sensors required for the Fine Pointing verification can be included, realizing an actual HIL simulation in a distributed testbed. The overall structure of this testbed is shown in Figure 7. The star tracker is located in a star simulator, which projects the sky view that reflects the simulated orientation [6]. To stimulate the gyroscopes, the satellite's EM is mounted into a highly precise turntable.

The simulation framework is the same as described in the previous section. However, with the gyroscope and star tracker in the loop, the simulation is not required to compute the model output for these sensors. Instead, the currently simulated state needs to be forwarded to the testbed components. For the star simulator, this happens via a user datagram protocol (UDP) connection. An MCU controls the turntable with a software stack similar to that of the satellite. Therefore, COMPASS is used here as well to transfer the state of the simulation via USB to the controller. It requires time-stamped information so that it can interpolate between the discrete updates it receives from the simulation.

The measured attitude $\overrightarrow{q_{st}}$ by the star tracker is directly fed into the ADCS via a wireless universal asynchronous receiver transmitter (UART) connection. The wireless communication adds an additional measurement delay, which will not be existent in orbit.

The turntable controller software is synchronized to the simulation relying on SNTP as well, allowing accurate timed movements of the mounted EM. The turntable has an angular range of $\pm 120°$ for the x and y axis. Around the z (inner) axis, it can perform unlimited rotation. This allows the simulation of various scenarios and complex rotations during the satellite overflights. However, due to its gimbal assembly, some scenarios may only be partially simulated due to the turntable running in a gimbal lock.

Like in the PIL, the torque is fed back to the simulation in this setting, which is not depicted in Figure 7 for simplicity. Thus, this testbed covers the whole chain from sensors to control output.

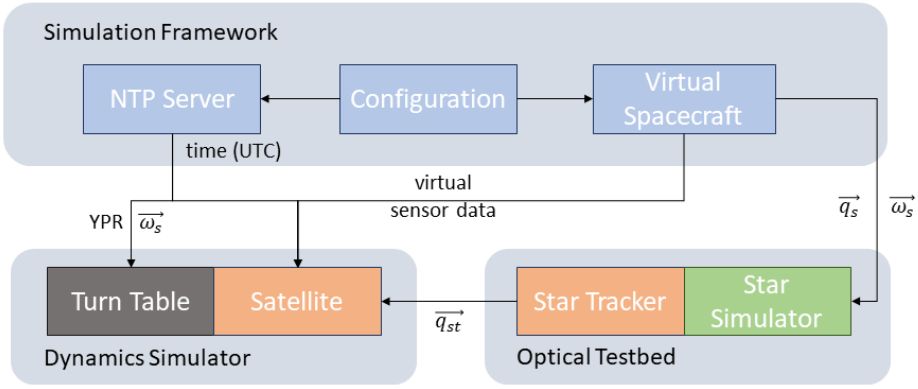

Figure 7: High-level distributed simulation architecture for HIL tests.

3 RESULTS

We evaluated the pointing error with the testbed described in Section 2.2.2 in various scenarios. For the HIL simulation, we selected a 550km Sun-synchronous orbit (SSO) with local time of the ascending node (LTAN) 11:00 to have similar orbit parameters as expected in QUBE-1. In this paper, we show the exemplary results for three different peak elevations: 30°, 60° and 90°. In order to calculate the pointing error during the overflights, the actual attitude computed in the simulation and the target attitude of the satellite are compared. The results are shown in Figure 8, 9 and 10. In addition to the pointing error, the attitude quaternion from the star tracker and the actual attitude quaternion from the simulation are plotted. In the 30° peak elevation scenario, the maximum pointing error was 0.4°. We could only run the first half of the overpass due to the turntable running in a gimbal lock. In the 60° peak elevation scenario, the maximum pointing error was 0.6° and in the 90° peak elevation scenario, there was about 1.25° pointing error during the highest elevation part. Comparing the pointing errors from the different scenarios shows that the pointing error increases with increasing peak elevations. This is expected as the dynamic increases with increasing elevation. In the 30° and 60° peak elevation scenarios the star tracker had no outages and the pointing error stayed well below the 1° pointing requirement. However, in the 90° peak elevation overflight, the 1° pointing requirement was not met during the highest elevation part. The reason for this is that the star tracker is operated outside the specifications and cannot cope with such high rotation rates, meaning that it can no longer provide attitude information. This is also visible in the plot in Figure 10, where no star tracker data is present. During the time when the star tracker has no fix, the filter propagates the state based on the gyroscope values, which leads to higher inaccuracies in attitude estimation.
Despite a good estimate of the gyroscope bias before losing the star tracker, an angular random walk cannot be avoided. As soon as the rotation rate decreases and the star tracker can get a fix again, the pointing error is reduced and stays well below 1°. Random short star tracker outages, as visible in Figure 10 at 01:05 h and 01:15 h, can be bridged by the gyroscope.
In all three scenarios, the MGSPF shows fast convergence. It is also able to deal with a lack of sensor data, and thus no update steps of the Kalman filter, for extended durations. It re-converges quickly as soon as data becomes available again. Table 1 shows a statistical analysis with the standard deviation σ_P of the resulting pointing error for the different scenarios after the initial pointing offset is corrected. In the 90° peak elevation scenario, the higher error reflects the loss of the star tracker fix during the high elevations of the overflight. Besides, the testbed also adds noise to the satellite that is not present in orbit. As the task of the turntable controller is to track the state of the simulation, the noise level correlates to the angular acceleration of the satellite. The faster the rotation rate changes, the more time the turntable requires to reach the new rate, resulting in slight deviations (control error) between

Table 1: Pointing error analysis during overpass, after correcting initial offset from course pointing.

scenario peak elevation	30°	60°	90°
σ_P	0.07°	0.10°	0.32°

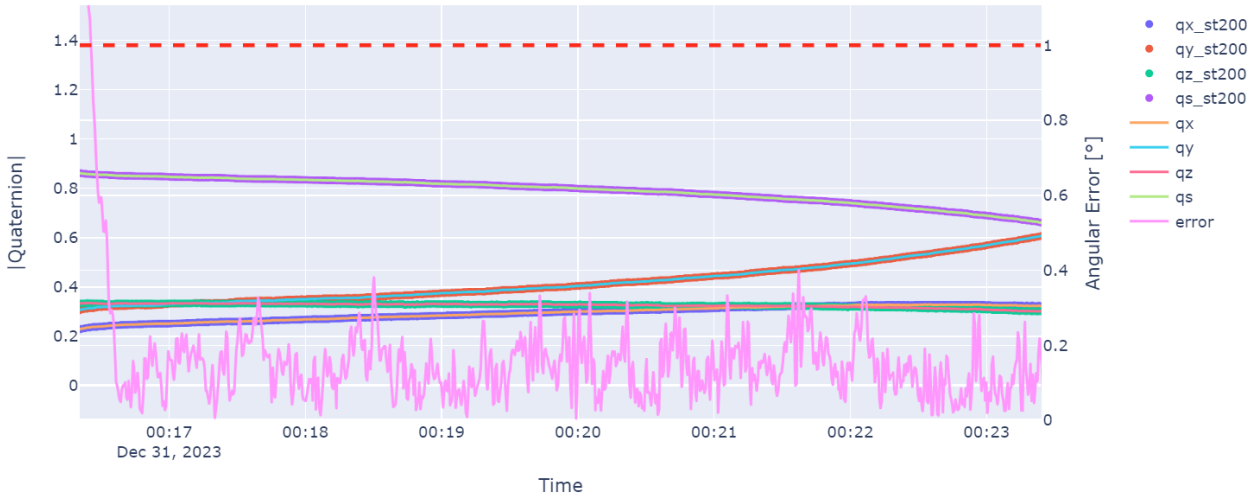

Figure 8: Pointing error for 30° peak elevation scenario.

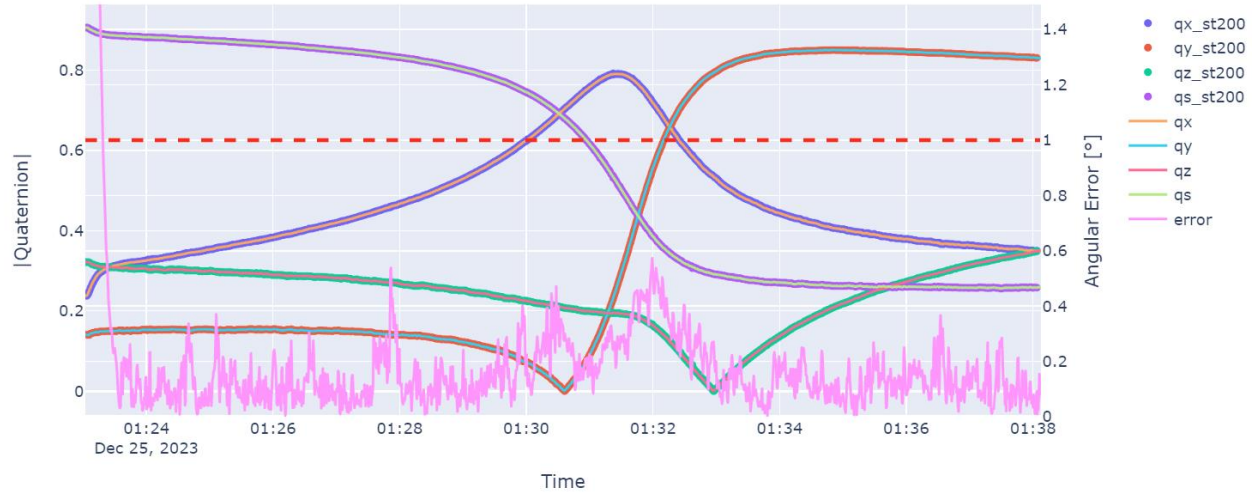

Figure 9: Pointing error for 60° peak elevation scenario.

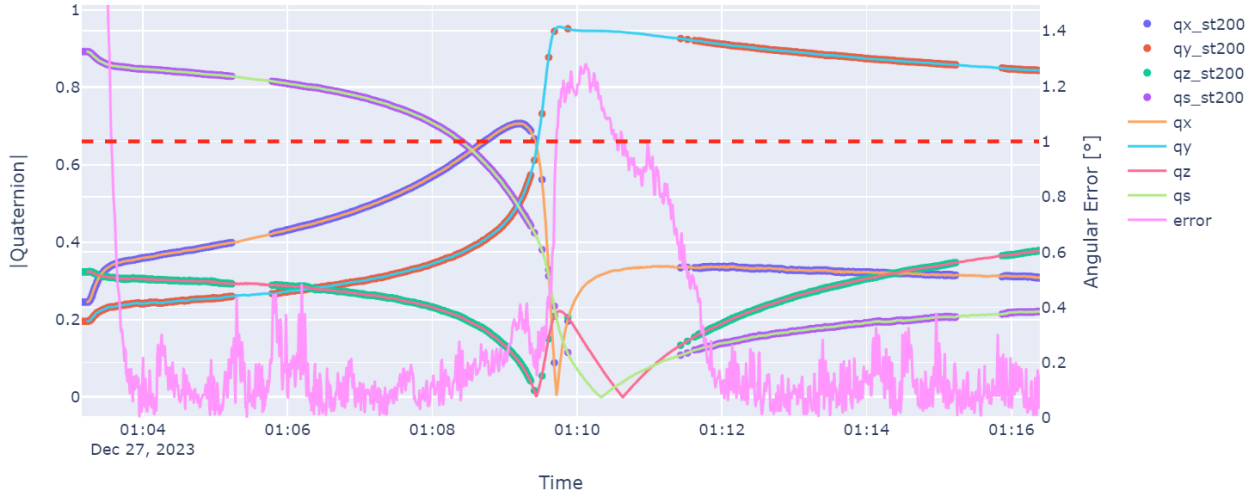

Figure 10: Pointing error for 90° peak elevation scenario.

the simulated and the actual state. This also contributes to the increased error in the 90° peak elevation scenario.

4 CONCLUSION

Despite the very small dimensions and the limited resources of a CubeSat, we demonstrate the achievement of the challenging ADCS pointing and tracking requirements on the ground needed to perform the QKD experiment. The tests demonstrated the reliability of the ADCS in maintaining precise pointing during the overflight.
Potential short star tracker dropouts can be compensated with the MGSPF without violating the 1° pointing accuracy, which increases the system's robustness. Even if more extended star tracker outages occur, it can be seen that the system nevertheless remains stable and quickly corrects the error in the orientation as soon as the star tracker provides an attitude again.
Our testbed not only serves as an essential platform for the reliable development and verification of ADCS systems on-ground but also as a potential enabler for future research projects. With QUBE-1 in orbit, the measured resulting pointing accuracy will be compared with the results in the HIL simulation to characterize the achieved accuracy. Beyond QUBE-1, this miniature ADCS system and the test equipment developments lay the foundation for upcoming missions in implementation stage, such as the QUBE-2 mission with improved laser equipment in an increased satellite, TOM - a formation of 3 nano-satellites for photogrammetric observations, CloudCT - a formation of 10 satellites to use computed tomography to improve characterization of clouds and LoLaSat - very low latency satellite communication system. All these missions are based on challenging attitude control requirements, requiring further extension of the test facilities towards formations and towards very low Earth orbits (VLEO), e.g., by models of additional external disturbances.

5 ACKNOWLEDGEMENT

The authors want to thank the German Federal Ministry of Education and Research (BMBF) for the funding within the IKT 2020 program, as well as the payload partners LMU Munich, MPL Erlangen, DLR-IKN and our ZfT-team, for the excellent cooperation in the QUBE-1 project.

6 REFERENCES

[1] J. Yin et al., “Satellite-based entanglement distribution over 1200 kilometers”, in *Science*, vol. 356, no. 6343, pp. 1140–1144, 2017

[2] I. Mammadov, J. Scharnagl, R. Haber, K. Schilling, “Quantum Key Distribution for Secure Communication by Nano-Satellites”, in *Proceedings of the 73rd International Astronautical Congress (IAC)*, Paris, IAC-22-B2.2.7

[3] L. Knips, M. Auer, A. Baliuka, Ö. Bayraktar, P. Freiwang, M. Grünefeld, R. Haber, N. Lemke, C. Marquardt, F. Moll, J. Pudelko, B. Rödiger, K. Schilling, C. Schmidt, and H. Weinfurter, “QUBE – Towards Quantum Key Distribution with Small Satellites,” in *Quantum 2.0*, Technical digest series / Optica Publishing Group, p. QTh3A.6, Optica Publishing Group, 2022.

[4] UNISEC Europe, “CubeSat Subsystem Interface Definition.” http://unisec-europe.eu/wordpress/wp-content/uploads/CubeSat-Subsystem-Interface-Standard-V2.0.pdf (accessed 2024-04-10).

[5] O. Ruf, M. v. Arnim, F. Kempf, R. Haber, L. Elsner, J. Dauner, S. Dombrovski, A. Kramer, and K. Schilling, “Advanced test environment for automated attitude control testing of fully integrated CubeSats on system level,” *CEAS Space Journal*, pp. 1–20, 2023.

[6] T. Petermann, L. Elsner, E. Jäger, M. von Arnim, K. Schilling, and G. Dietl, “A Distributed Hardware-in-the-Loop Testbed for Attitude Determination and Control Systems of Small Communication Satellites,” in *Proceedings of the AIAA/USU Conference on Small Satellites, SSC24-WP2-14*, 2024.

[7] F. L. Markley and J. L. Crassidis, *Fundamentals of spacecraft attitude determination and control*, vol. 33 of *Space technology library*. Springer, 2014.

[8] C. G. Mayhew, R. G. Sanfelice, and A. R. Teel, “Quaternion-based hybrid control for robust global attitude tracking,” *IEEE Transactions on Automatic Control*, vol. 56, no. 11, pp. 2555–2566, 2011.

[9] J. L. Crassidis, S. F. Andrews, F. L. Markley, and K. Ha, “Contingency designs for attitude determination of TRMM,” in *Flight Mechanics/Estimation Theory Symposium 1995*, pp. 419–433, May 1995.

[10] C. Fan and Z. You, “Highly efficient sigma point filter for spacecraft attitude and rate estimation” *Math. Probl. Eng.*, vol. 2009, pp. 1–23, 2009.

[11] “SNTP C client library for small IoT devices (MCU or small MPU).” www.freertos.org/coresntp (accessed 2024-04-10).

[12] CS-Group, “Orekit: an accurate and efficient core layer for space flight dynamics applications.” www.orekit.org (accessed 2024-04-10).

[13] “Hipparchus: a mathematics library.” www.hipparchus.org (accessed 2024-04-10).

[14] D. Gebre-Egziabher, G. H. Elkaim, J. D. Powell, and B. W. Parkinson, “Calibration of strapdown magnetometers in magnetic field domain,” *Journal of Aerospace Engineering*, vol. 19, no. 2, pp. 87–102, 2006.

[15] M. von Arnim, I. Mammadov, L. Draschka, J. Scharnagl, and K. Schilling, “The CloudCT formation of 10 nano-satellites for computed tomography to improve climate predictions,” in *Proceedings of the 73rd International Astronautical Congress (IAC)*, Sept. 2022